# Chiral criticality in the doped helimagnets $Mn_{1-y}Fe_ySi$

Sergey V. Grigoriev,[1] Evgeny V. Moskvin,[1] Vadim A. Dyadkin,[1] Daniel Lamago,[2,3] Thomas Wolf,[3] Helmut Eckerlebe,[4] and Sergey V. Maleyev[1]

[1]*Petersburg Nuclear Physics Institute, Gatchina, 188300 Saint-Petersburg, Russia*

[2]*Laboratoire Léon Brillouin, CEA Saclay, F-91191 Gif-sur-Yvette Cedex, France*

[3]*Karlsruher Institut für Technologie (KIT), Institut für Festkörperphysik, P.O. Box 3640, D-76021 Karlsruhe, Germany*

[4]*Helmholtz Zentrum Geesthacht, D-21502 Geesthacht, Germany*

(Received 8 April 2011; revised manuscript received 29 April 2011; published 21 June 2011)

The critical spin fluctuations in $Mn_{1-y}Fe_ySi$ compounds have been studied by means of ac-susceptibility measurements, polarized neutron small angle scattering, and spin echo spectroscopy. It is shown that these compounds undergo the transition from the paramagnetic to helimagnetic phase through continuous yet well distinguishable crossovers: (i) from paramagnetic to partially chiral and (ii) from partially chiral to highly chiral fluctuating state. The temperature crossovers are associated with the enhancing influence of the Dzyaloshinskii-Moria interaction close to $T_c$.

DOI: 10.1103/PhysRevB.83.224411 PACS number(s): 75.50.Cc, 61.05.fg, 75.40.−s, 76.60.Lz

## I. INTRODUCTION

The cubic B20-type (space group $P2_13$) compounds $Mn_{1-y}Fe_ySi$ with $y \in [0; 0.15]$ order in a spin helix structure with a small propagation vector $0.36 \leqslant k \leqslant 0.70\,\mathrm{nm}^{-1}$.[1,2] The spin helix structure is well interpreted within the Bak-Jensen (BJ) hierarchical model,[3] which implies the competition between the ferromagnetic spin exchange and antisymmetric Dzyaloshinskii-Moriya interaction (DMI), in its turn, caused by lack of an inverse symmetry in the arrangement of atoms.[3–5] The critical temperature of the compounds $T_c$ decreases with the Fe doping and approaches zero, discovering the quantum phase transition at $y_c \approx 0.15$. Additionally, the value of the helix wave vector increases significantly upon doping.[2] This study is aimed at demonstrating in detail the character and changes of the thermal phase transition upon its way to the quantum critical point at $y_c$.

The nature of the magnetic phase transition even in pure MnSi remains a subject of intensive debates.[6–11] The detailed study of the critical neutron scattering in pure MnSi had been reported in Ref. 7. It was shown that the scattering intensity of polarized neutrons above $T_c = 28.8$ K looks like half-spheres centered at the origin and oriented along the incident neutron polarization. This scattering was referred to the purely chiral spiral spin fluctuations with the wave vector $\mathbf{k}$ of the random orientation. The high degree of chirality of the fluctuations emphasizes a relative strength of the DMI. The sum of the intensities for two opposite polarizations forms an anisotropic sphere close to $T_c$ with weak spots, which below $T_c$ transform into the Bragg peaks assigned to the helical structure. The mean-field theory of the critical fluctuations based on the BJ model was proposed and shown to describe the experimental data very well.[7]

Later the closer look had revealed existence of a 100% chiral spin fluctuations within one K above $T_c$.[10] It was suggested that this region may be a candidate for the spontaneous fluctuating skyrmion phase[10] as was assumed in Ref. 8. Later in Ref. 11 we demonstrated in more detail, compared to Ref. 7, that existing experimental data are in good qualitative agreement with the conventional mean-field theory which catches principal symmetry features of the problem. To emphasize the generality of our approach, we note that the similar expression for the neutron cross section had been obtained for MnSi under applied pressure [see Eq. (10) in Ref. 7].

Moreover, we stress that the mean-field theory[7] accounting for the modifications of ferromagnetic fluctuations by DMI does not imply any texture of the fluctuating object (spiral or skyrmion). This theory describes the correlation length increasing on approaching $T_c$. Therefore the expressions derived in Refs. 7 and 11 for the susceptibility, the neutron cross section, and for the correlation functions must be valid for fluctuations of both spiral or skyrmion textures.

The magnetic properties of the doped compounds $Mn_{1-y}Fe_ySi$ as well as $Mn_{1-y}Co_ySi$ were recently studied by the measurements of the magnetization and ac susceptibility.[13] One of the remarkable findings in Ref. 13 is the temperature dependence of the saturation magnetization described by $m_s^2 = m_{s,0}^2(1 - T^2/T_m^2)$, where $T_m$ (denoted as $T_c$ in Ref. 13) is the critical temperature at which magnetization of the compound is extrapolated to zero. $T_m$ appears to be proportional to $(1 - \sqrt{y/y_c})$ with $y_c = 0.192$ for the $Mn_{1-y}Fe_ySi$ compounds. These findings confirm one of the conclusions made in Ref. 2 that ferromagnetic exchange representing the strongest energy scale of the system leads to the underlining ferromagnetic quantum critical point at $y_c$.

However, $T_m$ cannot be the transition temperature where the long-range helix structure appears, because the DMI modifies critical phenomena notably. At least two specific points can be extracted from the temperature dependence of ac susceptibility. The typical curve [see Fig. 1(a)] is characterized by the points of inflection of susceptibility at low temperature $T_c$ and at high temperature $T_{DM}$. These two points are denoted as $T_{c1}$ and $T_{c2}$ in Ref. 13, respectively. The true identification of these points is impossible without complementary data taken by small angle neutron diffraction. In this paper we fill the gap and demonstrate that $T_c$ ($T_{c1}$ in Ref. 13) corresponds to the transition into the helix phase and $T_{DM}$ ($T_{c2}$ in Ref. 13) implies a border within the paramagnetic phase, where DMI is large enough to change the character of the spin fluctuations from ferromagnetic to helix-like ones.

 

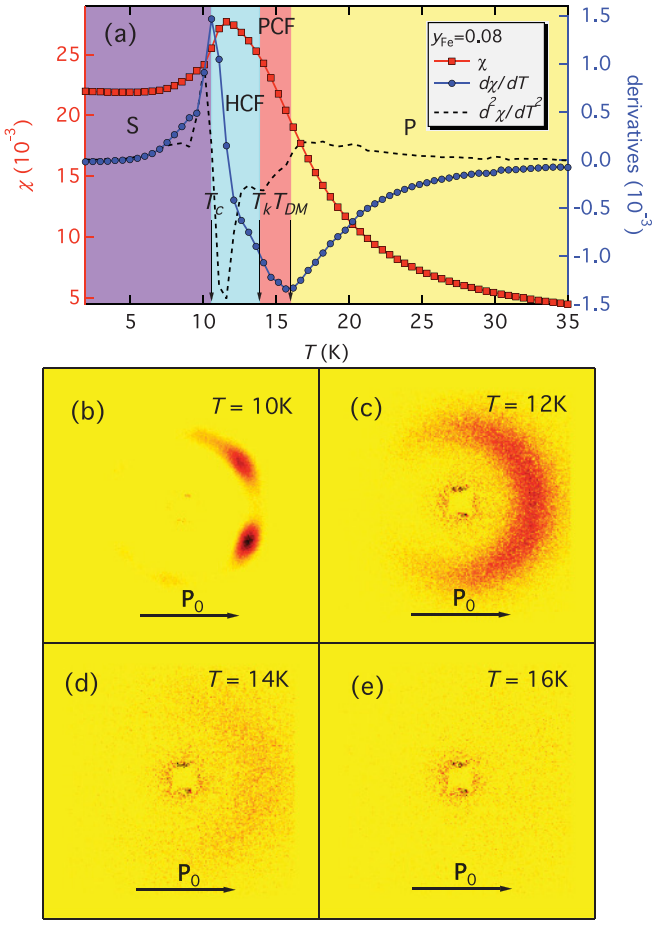


FIG. 1. (Color online) The sample with concentration $y = 0.08$. (a) The temperature dependencies $\chi$ (red squares), $d\chi/dT$ (blue circles), and $d^2\chi/dT^2$ (dashed line) in the magnetic field $H =$ 50 mT; four different temperature regions are shown (S, HCF, PCF, and P; see explanations in text). Four SANS maps corresponding to the shadowed/colored areas on the temperature scale are: (b) $T < T_c$, (c) $T_c \leqslant T \leqslant T_k$, (d) $T_k \leqslant T \leqslant T_{DM}$, and (e) $T > T_{DM}$.

## II. ac SUSCEPTIBILITY AND POLARIZED NEUTRON SCATTERING MEASUREMENTS

A series of $Mn_{1-y}Fe_ySi$ single crystals with $y = 0.0, 0.08,$ 0.09, 0.10, 0.12 have been studied using ac-susceptibility measurements at PPMS station in HZB, Berlin, Germany. Three of these samples with $y = 0.0, 0.08, 0.10$ were investigated by small angle polarized neutron scattering (SAPNS) at SANS-2 instrument of HZG (Geesthacht, Germany) and by Neutron Spin Echo at the wide angle NSE spectrometer SPAN at HZB (Berlin, Germany). We used an ac-susceptibility method to estimate the transition temperatures and SAPNS to examine the magnetic structure [Fig. 1(a) and Figs. 1(b)–1(e), respectively]. The examples of these measurements for the sample $Mn_{0.92}Fe_{0.08}Si$ are sketched in Fig 1. The temperature dependence of susceptibility $\chi$ is shown in Fig. 1(a). Here we also plot the first derivative of the susceptibility on the temperature $d\chi/dT$ to emphasize the inflection points $T_c$ and $T_{DM}$ on the $\chi(T)$ dependence. These inflection points divide the temperature scale into the three regions: (i) the low temperature spiral phase (S), (ii) high temperature paramagnetic phase (P), and (iii) the intermediate $T$ region between maximum and minimum of $d\chi/dT$ [Fig. 1(a)]. Yet another characteristic temperature, denoted as $T_k$ ($T^*$ in Ref. 2), has been distinguished from the analysis of the neutron scattering data (see below). This point corresponds in Fig. 1(a) to the local minimum of second derivative on the temperature $d^2\chi/dT^2$ within the range between $T_c$ and $T_{DM}$.

Bragg peaks on the SAPNS map in Fig. 1(b) manifest the low-$T$ spiral magnetic structure, which disappear at $T_c$. This temperature point determined from SAPNS data coincides with the temperature of maximum of $d\chi/dT$ in Fig. 1(a). Just above $T_c$ the diffuse critical scattering of the chiral fluctuations is formed as a half moon, centered at the structure position [Fig. 1(c)], similar to those observed in Ref. 7. This scattering depends strongly on the initial polarization. The asymmetric $P$-dependent scattering is a fingerprint of the single chirality of the spin helix that corresponds to the sign of the DMI. The radius of the ring of intensity observed above $T_c$ gives the length of the helix wave-vector $|\mathbf{k}| = 2\pi/d$ ($d$ is the spiral period). Its width gives the inverse correlation length of the spin fluctuations $\kappa$. The moon-like scattering image becomes blurred when temperature increases, $T > T_k$ [Fig. 1(d)]. Further increase of $T$ above $T_{DM}$ makes the moon-like scattering dissolve [Fig. 1(e)]. The quantitative analysis of the data is performed on the base of the mean-field theory of the critical neutron scattering for the cubic magnet with DMI.[7,11]

The neutron cross section for the paramagnetic phase ($T >$ $T_c$) is given in the following form:

$$\frac{d\sigma}{d\Omega} = \frac{r^2 T}{A} \frac{k^2 + \kappa^2 + Q^2 + 2\,\mathrm{sgn}(D) k \mathbf{Q}\cdot\mathbf{P}_0}{[(Q+k)^2+\kappa^2][(Q-k)^2+\kappa^2]}. \qquad (1)$$

Here $\mathbf{Q}$ is the scattering vector, $A$ is the spin wave stiffness at low $T$, $D$ is the Dzyaloshinskii constant, and $\mathbf{P}_0$ is the incident polarization of neutrons. In this expression we have neglected the weak anisotropic exchange which is essential in the very vicinity of $T_c$ only (see Refs. 7 and 11). Moreover, for doped compounds the local disorder smears the cubic anisotropy. On the other hand, the spiral structure with the period of order of 10 nm (and more) is very stable and not affected by the local disorder having well established length of $k$ over a macroscopic distances of the single crystal.

The cross section [Eq. (1)] has several features. (i) Due to the second term of the product in the denominator the scattering intensity should form a sphere of radius $Q = k$ with a width of $\kappa$. The scalar, not vector variables in $(Q-k)^2$, is a result of isotropic DMI in cubic ferromagnets. (ii) The intensity has the Lorentzian shape typical for critical fluctuations. (iii) The scattering intensity is strongly oriented along the incident neutron polarization since the numerator of Eq. (1) is maximal at $\mathbf{P}_0 \uparrow\uparrow \mathbf{Q}$ and it is minimal at $\mathbf{P}_0 \uparrow\downarrow \mathbf{Q}$. The DMI is responsible for this kind of scattering.

One can estimate the chirality of the critical fluctuations via measurement of the polarization of the scattering:

$$P_s(Q) = \frac{\sigma(\mathbf{P}_0) - \sigma(-\mathbf{P}_0)}{\sigma(\mathbf{P}_0) + \sigma(-\mathbf{P}_0)} = -\frac{2kQP_0\cos\phi}{Q^2+k^2+\kappa^2}, \qquad (2)$$

where $\phi$ is the angle between $\mathbf{P}_0$ and $\mathbf{Q}$ and we use Eq. (1) to estimate its value via parameters $Q$, $k$, and $\kappa$.

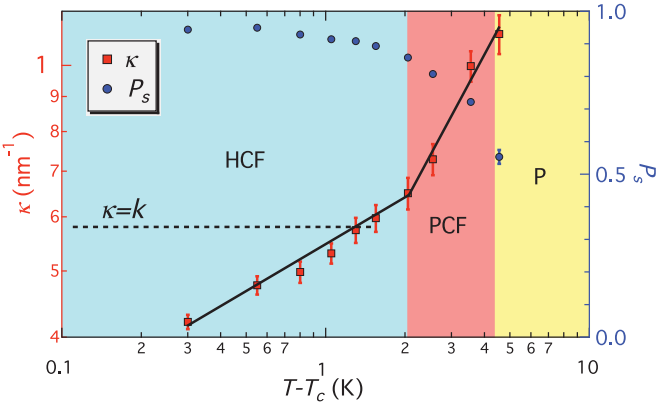


FIG. 2. (Color online) The inverse correlation length $\kappa$ (squares) and the polarization $P_s$ (circles) as a function of the temperature $T - T_c$ for $Mn_{0.92}Fe_{0.08}Si$. Straight lines are guides to the eyes.

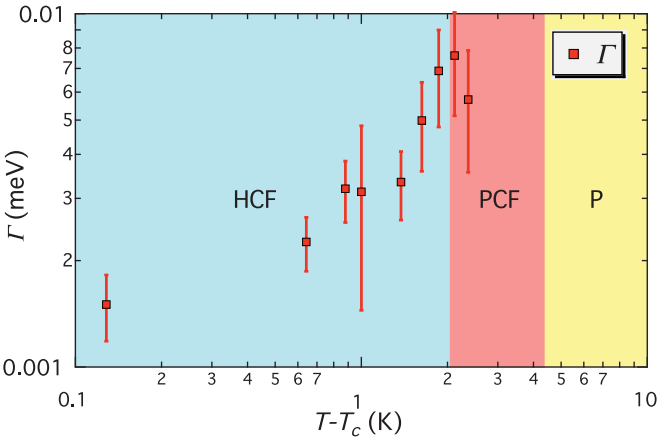


FIG. 3. (Color online) The relaxation rate of the fluctuations Γ as a function of the temperature $T - T_c$ for $Mn_{0.92}Fe_{0.08}Si$.

The whole set of the experimental data obtained by polarized SANS was fitted to Eq. (1). The inverse correlation length $\kappa$ and the position of the maximum $k$ were obtained as a result of the fit. The temperature dependence of the inverse correlation length $\kappa$ for $Mn_{0.92}Fe_{0.08}Si$ is shown in Fig. 2. The meaningful values for $\kappa$ had been possible to extract from the data in the temperature range $T_c < T < T_{DM}$ [corresponding to the middle area in Fig. 1(a)], where $\kappa$ changes from $2k$ at $T = T_{DM}$ to $(2/3)k$ at $T_c$. The temperature dependence of $\kappa$ in the log-log scale (Fig. 2) exhibits a crossover at $T = T_k$, where $\kappa \simeq k$.

As it is well seen in Fig. 2 and was also noted in Refs. 7, 10, and 11 the polarization $P_s(Q = k)$ is close to 1 in the range $T_c \leqslant T \leqslant T_k$, showing highly chiral fluctuating state within this range. The polarization $P_s$ decreases smoothly upon increase of temperature above $T_k$. We refer to this change in the temperature behavior of $P_s$ as to the crossover from highly chiral fluctuating (HCF) phase with $\kappa < k$ to the partially chiral (PCF) phase with $\kappa > k$. Thus, this crossover in $T$ dependence of $P_s$ is well correlated with the crossover behavior of $\kappa(T)$.

To study the critical dynamics in these compounds we have used the paramagnetic neutron spin echo (NSE) technique. The temperature stabilization accuracy was $\Delta T = 0.01$ K. All NSE spectra were normalized by the resolution function of the spectrometer, determined at $T = 2$ K well below $T_c$, where there is no inelastic contribution to the spin-echo signal visible by this technique. The intermediate scattering function $S(Q,t)$ was measured at the magnetic Bragg point $\mathbf{Q} = \mathbf{k}$ along $\langle 111 \rangle$ crystal axis within the chiral fluctuating phase $T_c \leqslant T \leqslant T_k$. The temperature dependence of the relaxation rate Γ is shown in Fig. 3. It decreases upon approaching $T_c$ in the HC range.

### III. $(T - y)$ PHASE DIAGRAM

To underline a typical shape of the ac-susceptibility data we give in Fig. 4 three other examples of the temperature dependencies $\chi$, $d\chi/dT$, and $d^2\chi/dT^2$ for the samples with $y = 0.09$, 0.10, and 0.12. The compounds undergo the transition from the paramagnetic (P) phase (with Curie-Weiss dependence at $T > T_{DM}$) to spiral (S) phase ($T < T_c$) through two intermediate regions PCF phase ($T_k < T < T_{DM}$) and

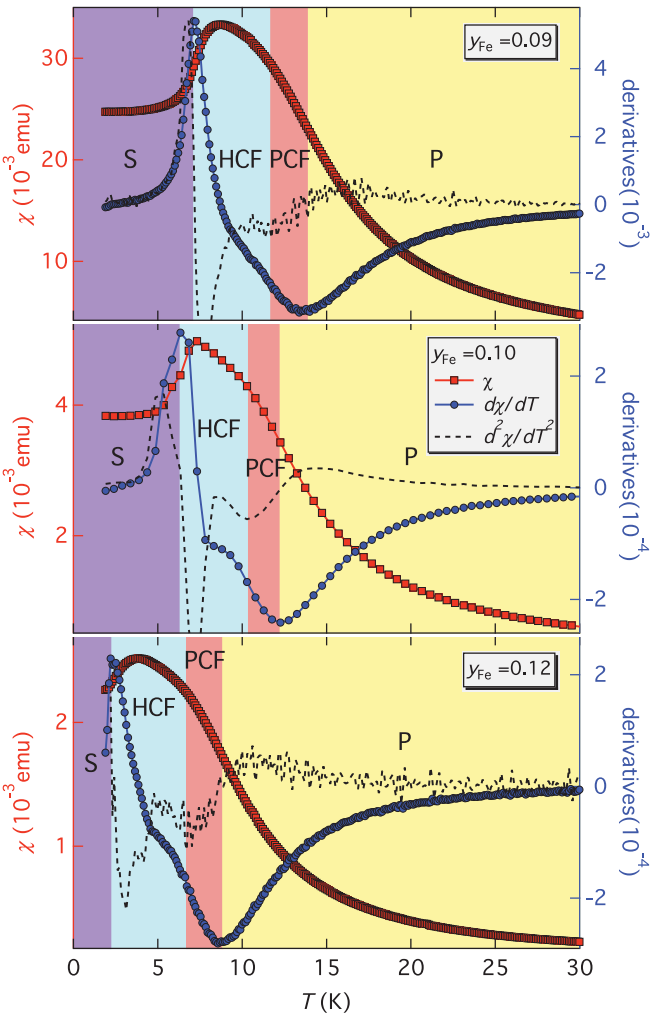


FIG. 4. (Color online) ac-susceptibility measurements. The same temperature dependencies as in Fig. 1(a) but for other three concentrations: $y = 0.09$, 0.10, and 0.12 on the upper, the middle, and the lower graphs, respectively. Four different temperature regions, S, HC, PC and P, are also shown, colored the same as in Fig. 1(a).

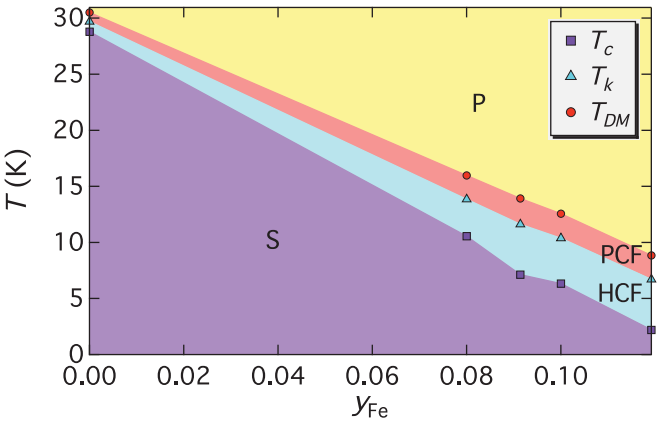


FIG. 5. (Color online) Concentration dependencies of the critical temperature $T_c$ and the crossovers points $T_{DM}$ and $T_k$ for $Mn_{1-y}Fe_ySi$ compounds. The inset shows the temperature dependencies $\chi$, $d\chi/dT$, and $d^2\chi/dT^2$ in the magnetic field $H = 50$ mT for the sample with $y = 0.10$.

HCF phase ($T_c \leqslant T \leqslant T_k$). We have to stress that the transition is the only one at $T = T_c$, and the other temperature points correspond to crossovers.

From the ac-susceptibility and SAPNS measurements we have established three specific temperature points ($T_c$, $T_k$, and $T_{DM}$), which are plotted in Fig. 5 on the $(T - y)$ phase diagram.

The scenario of the phase transition in the $Mn_{1-y}Fe_ySi$ compounds thus can be determined by the relation between the inverse correlation length $\kappa$ and the spiral wave vector $k$. In the high temperature range ($T > T_{DM}$) the critical fluctuations are limited by $\kappa > 2k$ or $\xi < \pi/k = d/2$, where $d$ is the spiral period. For these fluctuations noncollinearity is not essential and they are close to the fluctuations of the conventional ferromagnet. In turn, the ac susceptibility demonstrates Curie-Weiss behavior at $T > T_{DM}$. The transition through the inflection point of susceptibility at $T_{DM}$ leads to the PC state with $k < \kappa < 2k$, or with the correlation length in real space $d/2 < \xi < d$. The full $2\pi$ twist of the helix is not completed yet within these fluctuations. This results in rather low degree of chirality of such fluctuations. Further down on temperature ($T_c < T < T_k$), when the full $2\pi$ twist of the helix is well established within the fluctuations ($\kappa < k$), the highly

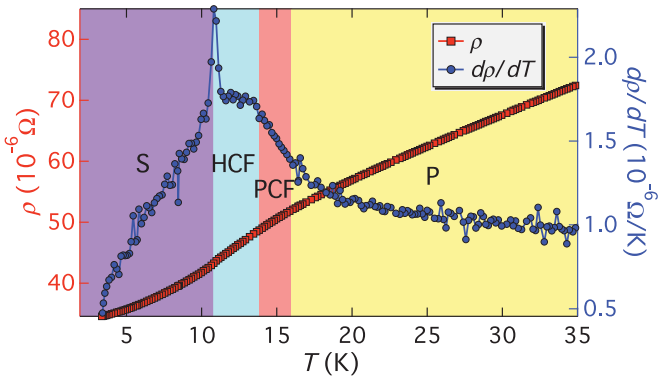


FIG. 6. (Color online) The temperature dependence of resistivity $\rho$ and its first derivative $d\rho/dT$ for $Mn_{0.92}Fe_{0.08}Si$.

TABLE I. Parameters of $Mn_{1-y}Fe_ySi$ compounds for the HCF state.

| $y$ | $T_c$ (K) | $k$ (nm$^{-1}$) | $\kappa$ (nm$^{-1}$) | $\Gamma$ ($\mu$eV) |
|---|---|---|---|---|
| 0 | 29.0(1) | 0.40 | $0.15 \leqslant \kappa \leqslant 0.3$ | 1–2 |
| 0.08 | 10.8(4) | 0.58 | $0.4 \leqslant \kappa \leqslant 0.6$ | 2–5 |
| 0.10 | 6.5(5) | 0.64 | $0.5 \leqslant \kappa \leqslant 0.7$ | 2–4 |

chiral fluctuating phase appears. The temperature dependencies of both $\kappa$ and $P_s$ demonstrate the crossover at $\kappa \sim k$. The crossover is compatible with the theory.[11] The global transition is completed at $T_c$ where the solid spiral structure arises.

Importance of the proposed delimitation of the $(T - y)$ phase diagram is demonstrated in the temperature dependencies of the other, nonmagnetic physical properties of these compounds. Figure 6 shows the temperature dependence of the resistivity of the compound with $y = 0.08$. The first derivative $d\rho/dT$ enlightens the changes undergoing with the resistivity upon the temperature change. The critical temperature $T_c$ is marked by a sharp peak of $d\rho/dT$. A plato in $T$ dependence appears between $T_c$ and $T_k$, that is, in the HCF state. The function decreases linearly in the PCF state in the range between $T_k$ and $T_{DM}$. Thus the shape of the $T$ dependence is very well correlated with four regions in the magnetic properties of the compounds. Interesting to note that this $T$ dependence duplicates temperature behavior of the specific heat and thermal expansion coefficient.[9]

Accounting for the importance of the HCF state between $T_c$ and $T_k$ for the physical properties of these compounds, we have collected in Table I the characteristic values of the inverse correlation length $\kappa$ and energy $\Gamma$ of the critical fluctuations for different concentrations $y$. As seen in Table I, the critical temperature $T_c$ decreases with concentration $y$ while the helix wave vector $k$ increases. These two quantities are interconnected via the two main energy scales: the DMI and the ferromagnetic exchange interaction (see for details Ref. 2). The inverse correlation length $\kappa$ within the HCF phase is clearly restricted by $\kappa_{\min}(T_c) \leqslant \kappa \leqslant \kappa_{\max}(T_k) \simeq k$. The relaxation rate $\Gamma$ changes weakly within the HCF state for an individual compound. For all compounds under study it can be satisfactory described by following empirical relation $\Gamma \sim T_c(ka)^x$ with $x \approx 4$. However, the dynamical properties of these compounds in the critical range have not been studied theoretically yet.

## IV. CONCLUSIONS

The scenario of the phase transition in the $Mn_{1-y}Fe_ySi$ compounds is described. Three characteristic points are identified on the basis of combined analysis of the temperature dependence of ac susceptibility and polarized SANS data. The upper one corresponds to the crossover from paramagnetic to partially chiral fluctuating state at $T_{DM}$, where the inverse correlation length $\kappa \approx 2k$, the lower one corresponds to the transition to the spin helix structure at $T_c$. The intermediate crossover to the highly chiral fluctuating phase is observed at the inflection point $T_k$, where $\kappa \approx k$. This scenario is clearly reflected in the nonmagnetic properties of these compounds,

such as resistivity, etc. The critical range from $T_{DM}$ to $T_c$ increases upon increase of $y$ as system approaches the quantum critical point at $y \approx 0.15$. Further study of the magnetic structure and spin fluctuations around the quantum critical point using small angle neutron scattering would be of great interest.

**ACKNOWLEDGMENTS**

The PNPI team acknowledges GKSS for their hospitality. The work is partly supported by the RFBR Projects No. 09-02-01023-à, No. 10-02-01205-a and Goskontrakt No 02.740.11.0874.

[1]Y. Nishihara, S. Waki, and S. Ogawa, Phys. Rev. B **30**, 32 (1984).

[2]S. V. Grigoriev, V. A. Dyadkin, E. V. Moskvin, D. Lamago, T. Wolf, H. Eckerlebe, and S. V. Maleyev, Phys. Rev. B **79**, 144417 (2009).

[3]P. Bak and M. H. Jensen, J. Phys. C **13**, L881 (1980).

[4]I. E. Dzyaloshinskii, Zh. Eksp. Teor. Fiz. **46**, 1420 (1964) [Sov. Phys. JETP **19**, 1228 (1964)].

[5]O. Nakanishi, A. Yanase, A. Hasegawa, and M. Kataoka, Solid State Commun. **35**, 995 (1980).

[6]B. Roessli, P. Böni, W. E. Fischer, and Y. Endoh, Phys. Rev. Lett. **88**, 237204 (2002).

[7]S. V. Grigoriev, S. V. Maleyev, A. I. Okorokov, Y. O. Chetverikov, R. Georgii, P. Boni, D. Lamago, H. Eckerlebe, and K. Pranzas, Phys. Rev. B **72**, 134420 (2005).

[8]U. K. Rössler, A. N. Bogdanov, and C. Pfleiderer, Nature (London) **442**, 797 (2006).

[9]S. M. Stishov, A. E. Petrova, S. Khasanov, G. K. Panova, A. A. Shikov, J. C. Lashley, D. Wu, and T. A. Lograsso, Phys. Rev. B **76**, 052405 (2007).

[10]C. Pappas, E. Lelièvre-Berna, P. Falus, P. M. Bentley, E. Moskvin, S. Grigoriev, P. Fouquet, and B. Farago, Phys. Rev. Lett. **102**, 197202 (2009).

[11]S. V. Grigoriev, S. V. Maleyev, E. V. Moskvin, V. A. Dyadkin, P. Fouquet, and H. Eckerlebe, Phys. Rev. B **81**, 144413 (2010).

[12]S. Tewari, D. Belitz, and T. R. Kirkpatrick, Phys. Rev. Lett. **96**, 047207 (2006).

[13]A. Bauer, A. Neubauer, C. Franz, W. Münzer, M. Garst, and C. Pfleiderer, Phys. Rev. B **82**, 064404 (2010).